# Gene-DML: Dual-Pathway Multi-Level Discrimination for Gene Expression Prediction from Histopathology Images

## Supplementary Material

This supplementary material complements the main manuscript by providing detailed information and additional support. It is structured as follows:

**Appendix A: Additional Cross-validation Performance** - Provides the MAE results on three ST datasets to further evaluate the cross-validation performance of Gene-DML.

**Appendix B: Additional Generalization Performance** - Provides the generalization performance of Gene-DML compared to TRIPLEX across 2 additional unseen skin cancer Visium ST data.

**Appendix C: Additional Ablation Study** - Provides the effectiveness of each key component in the model Gene-DML and hyperparameter configurations of $k$, $\lambda$, and $\tau_{I\text{-}G}$ on datasets HER2ST and STNet.

**Appendix D: Additional Visualization** - Provides additional sample visualizations of gene expression prediction of cancer biomarker genes across three ST datasets.

**Appendix E: Additional Implementation Details** - Provides specific 250 genes selected for each dataset to evaluate PCC(A) metric, the average of the Pearson Correlation Coefficient of 250 selected genes, of the Gene-DML.

## A. Additional Cross-validation Performance

Tab. 1 demonstrates a cross-validation comparison of mean absolute error (MAE) across three spatial transcriptomics datasets, HER2ST, STNet, and skinST, benchmarking our proposed method, Gene-DML, against several state-of-the-art baseline methods. Gene-DML consistently achieves the best performance across all datasets. Specifically, on HER2ST, Gene-DML attains an MAE of 0.350, outperforming the second-best method, TRIPLEX (0.362), with 0.012 improvement. On STNet, Gene-DML achieves an MAE of 0.327, improving upon Hist2ST (0.333) by 0.006. On skinST, Gene-DML reaches an MAE of 0.350, outperforming TRIPLEX (0.404) with a substantial 0.054 improvement. These consistent gains across diverse datasets highlight the effectiveness of the dual-dimensional multi-level discrimination framework in capturing semantically aligned multi-level cross-modal representations.

| Model | HER2ST | STNet | skinST |
|---|---|---|---|
| | MAE↓ | MAE↓ | MAE↓ |
| ST-Net [2] | $0.389 \pm 0.03$ | $0.349 \pm 0.02$ | $0.428 \pm 0.05$ |
| HistoGene [4] | $0.428 \pm 0.07$ | $0.335 \pm 0.04$ | $0.415 \pm 0.07$ |
| Hist2ST [8] | $0.413 \pm 0.07$ | $\underline{0.333} \pm 0.02$ | $0.924 \pm 0.29$ |
| EGN [7] | $0.377 \pm 0.04$ | $0.337 \pm 0.02$ | $0.418 \pm 0.06$ |
| BLEEP [6] | $0.401 \pm 0.03$ | $0.369 \pm 0.02$ | $0.430 \pm 0.04$ |
| TRIPLEX [1] | $\underline{0.362} \pm 0.05$ | $0.343 \pm 0.02$ | $\underline{0.404} \pm 0.07$ |
| M2OST [5] | $0.421 \pm 0.02$ | $0.362 \pm 0.01$ | $0.418 \pm 0.03$ |
| Gene-DML | $\mathbf{0.350} \pm 0.04$ | $\mathbf{0.327} \pm 0.02$ | $\mathbf{0.350} \pm 0.05$ |

Table 1. Additional comparison of cross-validation experiments with baselines on metric MAE. The **best results** are in bold; the second-best results are underlined.

| Model | NCBI463 | | | | NCBI464 | | | |
|---|---|---|---|---|---|---|---|---|
| | MSE↓ | MAE↓ | PCC(A)↑ | PCC(H)↑ | MSE↓ | MAE↓ | PCC(A)↑ | PCC(H)↑ |
| TRIPLEX | 0.342 | 0.478 | 0.103 | 0.360 | 0.416 | 0.538 | 0.091 | 0.261 |
| **Gene-DML (ours)** | **0.253** | **0.413** | **0.109** | **0.377** | **0.292** | **0.445** | **0.140** | **0.441** |

Table 2. Generalization performance on NCBI463 and NCBI464.

## B. Additional Generalization Performance

We further extend the evaluation by adding two skin cancer Visium datasets (NCBI463 and NCBI464) [3] to verify the skinST pre-trained models. Tab. 2 further underscores Gene-DML's outstanding generalization performance, achieving state-of-the-art results across all evaluation metrics MSE, MAE, PCC(A), and PCC(H).

## C. Additional Ablation Study

To evaluate the dual-pathway multi-level discrimination framework, Gene-DML, we perform an ablation study by adding each discrimination pathway sequentially together with their corresponding key components: the global-scale representation and feature grouping, and report the results of MSE, MAE, PCC(A), and PCC(H) metrics. Tab. 3 and Tab. 7 demonstrate the effectiveness of each component in Gene-DML on datasets HER2ST and STNet. They show that, by removing both pathways, a plain bimodal framework yields the weakest performance. By incorporating the multi-scale instance-level discrimination pathway and cross-level instance-group discrimination pathway, respectively, a significant improvement is achieved.

For the hyperparameter configuration of $k$ (number of groups), $\lambda$ (the weight of instance-group cross-level loss), and $\tau_{I\text{-}G}$ (the temperature of instance-group similarity cal-

culation), Tab. 4, Tab. 5, and Tab. 6 respectively present the result of the dataset HER2ST. As for the STNet dataset, please refer to Tab. 8, Tab. 9, and Tab. 10.

Overall, all these results show that while $k = 18$ and $\lambda = 0.8$ with $\tau_{I\text{-}G} = 0.07$, Gene-DML could achieve optimal performance across all evaluation metrics, thus setting it as the default configuration for HER2ST dataset; besides, $k = 25$ and $\lambda = 0.8$ with $\tau_{I\text{-}G} = 0.07$ are set as the default configuration for STNet dataset.

| Multi-scale I-L Dis. | Global Rep. | Cross-level I-G Dis. | Feature Grouping | MSE↓ | MAE↓ | PCC(A)↑ | PCC(H)↑ |
|---|---|---|---|---|---|---|---|
| ✗ | ✗ | ✗ | ✗ | 0.340 | 0.445 | 0.231 | 0.392 |
| ✓ | ✓ | ✗ | ✗ | 0.298 | 0.412 | 0.301 | 0.463 |
| ✗ | ✗ | ✓ | ✓ | 0.270 | 0.415 | 0.302 | 0.482 |
| ✓ | ✗ | ✓ | ✓ | 0.221 | 0.364 | 0.282 | 0.416 |
| ✓ | ✓ | ✓ | ✗ | 0.230 | 0.360 | 0.303 | 0.400 |
| ✓ | ✓ | ✓ | ✓ | **0.210** | **0.350** | **0.331** | **0.541** |

Table 3. Ablation study on components of the dataset HER2ST. Abbreviations in this table include instance-level discrimination (I-L Dis.), global-scale representation (Global Rep.) and instance-group discrimination (I-G Dis.).

| $k$ | MSE↓ | MAE↓ | PCC(A)↑ | PCC(H)↑ |
|---|---|---|---|---|
| 15 | 0.242 | 0.371 | 0.299 | 0.510 |
| 16 | 0.235 | 0.370 | 0.323 | 0.536 |
| 18 | **0.210** | **0.350** | **0.331** | **0.541** |
| 20 | 0.250 | 0.397 | 0.320 | 0.514 |

Table 4. Ablation study on the number of $k$-groups in the feature grouping process on the dataset HER2ST.

| $\lambda$ | MSE↓ | MAE↓ | PCC(A)↑ | PCC(H)↑ |
|---|---|---|---|---|
| 0.3 | 0.231 | 0.369 | 0.326 | 0.525 |
| 0.5 | 0.213 | 0.359 | 0.331 | 0.532 |
| 0.8 | **0.210** | **0.350** | **0.331** | **0.541** |
| 1 | 0.215 | 0.360 | 0.322 | 0.537 |

Table 5. Ablation study on the weight of instance-group loss $\lambda$ on the dataset HER2ST. $\lambda = 1$ indicates that the weight of instance-group loss is not applied in the experimental setting.

| $\tau_{I\text{-}G}$ | MSE↓ | MAE↓ | PCC(A)↑ | PCC(H)↑ |
|---|---|---|---|---|
| 0.05 | 0.220 | 0.355 | 0.329 | 0.532 |
| 0.07 | **0.210** | **0.350** | **0.331** | **0.541** |
| 0.1 | 0.238 | 0.371 | 0.320 | 0.534 |

Table 6. Ablation study on the temperature of instance-group similarity calculation $\tau_{I\text{-}G}$ on the dataset HER2ST.

| Multi-scale I-L Dis. | Global Rep. | Cross-level I-G Dis. | Feature Grouping | MSE↓ | MAE↓ | PCC(A)↑ | PCC(H)↑ |
|---|---|---|---|---|---|---|---|
| ✗ | ✗ | ✗ | ✗ | 0.269 | 0.440 | 0.160 | 0.233 |
| ✓ | ✓ | ✗ | ✗ | 0.246 | 0.400 | 0.211 | 0.308 |
| ✗ | ✗ | ✓ | ✓ | 0.232 | 0.379 | 0.198 | 0.301 |
| ✓ | ✗ | ✓ | ✓ | 0.184 | 0.339 | 0.227 | 0.361 |
| ✓ | ✓ | ✓ | ✗ | 0.188 | 0.338 | 0.216 | 0.309 |
| ✓ | ✓ | ✓ | ✓ | **0.179** | **0.327** | **0.237** | **0.384** |

Table 7. Ablation study on components of the dataset STNet. Abbreviations in this table include instance-level discrimination (I-L Dis.), global-scale representation (Global Rep.) and instance-group discrimination (I-G Dis.).

| $k$ | MSE↓ | MAE↓ | PCC(A)↑ | PCC(H)↑ |
|---|---|---|---|---|
| 80 | 0.185 | 0.331 | 0.236 | 0.376 |
| 90 | **0.179** | **0.327** | **0.237** | **0.384** |
| 100 | 0.188 | 0.332 | 0.230 | 0.368 |

Table 8. Ablation study on the number of $k$-groups in the feature grouping process on the dataset STNet.

| $\lambda$ | MSE↓ | MAE↓ | PCC(A)↑ | PCC(H)↑ |
|---|---|---|---|---|
| 0.5 | 0.205 | 0.350 | 0.200 | 0.349 |
| 0.8 | **0.179** | **0.327** | **0.237** | **0.384** |
| 1 | 0.202 | 0.345 | 0.228 | 0.361 |

Table 9. Ablation study on the weight of instance-group loss $\lambda$ on the dataset STNet. $\lambda = 1$ indicates that the weight of instance-group loss is not applied in the experimental setting.

| $\tau_{I\text{-}G}$ | MSE↓ | MAE↓ | PCC(A)↑ | PCC(H)↑ |
|---|---|---|---|---|
| 0.05 | 0.201 | 0.365 | 0.222 | 0.375 |
| 0.07 | **0.179** | **0.327** | **0.237** | **0.384** |
| 0.1 | 0.186 | 0.331 | 0.235 | 0.382 |

Table 10. Ablation study on the temperature of instance-group similarity calculation $\tau_{I\text{-}G}$ on the dataset STNet.

## D. Additional Visualizations

In this section, we provide additional visualizations of the gene expression prediction results, which are normalized into the range $[0, 1]$, of the breast cancer biomarker genes GNAS and FASN. Fig. 1 demonstrates the spatial gene expression prediction for GNAS and FASN on the HER2ST dataset. Each row displays a WSI sample alongside the ground-truth expression map and predictions from TRIPLEX (the method achieved the second-best result evaluated in Tab. 1 of Sec. 4.2.) and the proposed Gene-DML. Across both genes and multiple WSI samples, Gene-DML consistently produces spatial expression patterns that are visually closer to the ground truth and quantitatively higher in performance, as reflected by the reported Pearson correlation coefficients in parentheses. The same conclusion holds

for Fig. 2, which shows the spatial gene expression prediction results on the dataset STNet, further validating the strong gene expression prediction capacity of Gene-DML.

## E. Additional Implementation Details

To ensure fairness, following TRIPLEX [1], we utilize the various 250 selected genes for each dataset, *i.e.*, HER2ST, STNet, and skinST, that are related to morphology in histopathology to evaluate the performance of gene expression prediction. For the results of the MSE, MAE, and PCC(A) metrics in the cross-validation experiments, the same 250 genes were utilized for both the training and testing processes. Fig. 3, Fig. 4, and Fig. 5 demonstrate the 250 genes exploited to predict gene expression profiles on datasets HER2ST, STNet, and skinST, respectively.

## References


[1] Youngmin Chung, Ji Hun Ha, Kyeong Chan Im, and Joo Sang Lee. Accurate spatial gene expression prediction by integrating multi-resolution features. In *Proceedings of the IEEE/CVF Conference on Computer Vision and Pattern Recognition*, pages 11591–11600, 2024. 1, 3

[2] Bryan He, Ludvig Bergenstråhle, Linnea Stenbeck, Abubakar Abid, Alma Andersson, Åke Borg, Jonas Maaskola, Joakim Lundeberg, and James Zou. Integrating spatial gene expression and breast tumour morphology via deep learning. *Nature biomedical engineering*, 4(8):827–834, 2020. 1

[3] Guillaume Jaume, Paul Doucet, Andrew Song, Ming Yang Lu, Cristina Almagro Pérez, Sophia Wagner, Anurag Vaidya, Richard Chen, Drew Williamson, Ahrong Kim, et al. Hest-1k: A dataset for spatial transcriptomics and histology image analysis. *Advances in Neural Information Processing Systems*, 37: 53798–53833, 2024. 1

[4] Minxing Pang, Kenong Su, and Mingyao Li. Leveraging information in spatial transcriptomics to predict super-resolution gene expression from histology images in tumors. *BioRxiv*, pages 2021–11, 2021. 1

[5] Hongyi Wang, Xiuju Du, Jing Liu, Shuyi Ouyang, Yen-Wei Chen, and Lanfen Lin. M2ost: Many-to-one regression for predicting spatial transcriptomics from digital pathology images. In *Proceedings of the AAAI Conference on Artificial Intelligence*, pages 7709–7717, 2025. 1

[6] Ronald Xie, Kuan Pang, Sai Chung, Catia Perciani, Sonya MacParland, Bo Wang, and Gary Bader. Spatially resolved gene expression prediction from histology images via bimodal contrastive learning. *Advances in Neural Information Processing Systems*, 36:70626–70637, 2023. 1

[7] Yan Yang, Md Zakir Hossain, Eric A Stone, and Shafin Rahman. Exemplar guided deep neural network for spatial transcriptomics analysis of gene expression prediction. In *Proceedings of the IEEE/CVF Winter Conference on Applications of Computer Vision*, pages 5039–5048, 2023. 1

[8] Yuansong Zeng, Zhuoyi Wei, Weijiang Yu, Rui Yin, Yuchen Yuan, Bingling Li, Zhonghui Tang, Yutong Lu, and Yuedong Yang. Spatial transcriptomics prediction from histology jointly through transformer and graph neural networks. *Briefings in Bioinformatics*, 23(5):bbac297, 2022. 1

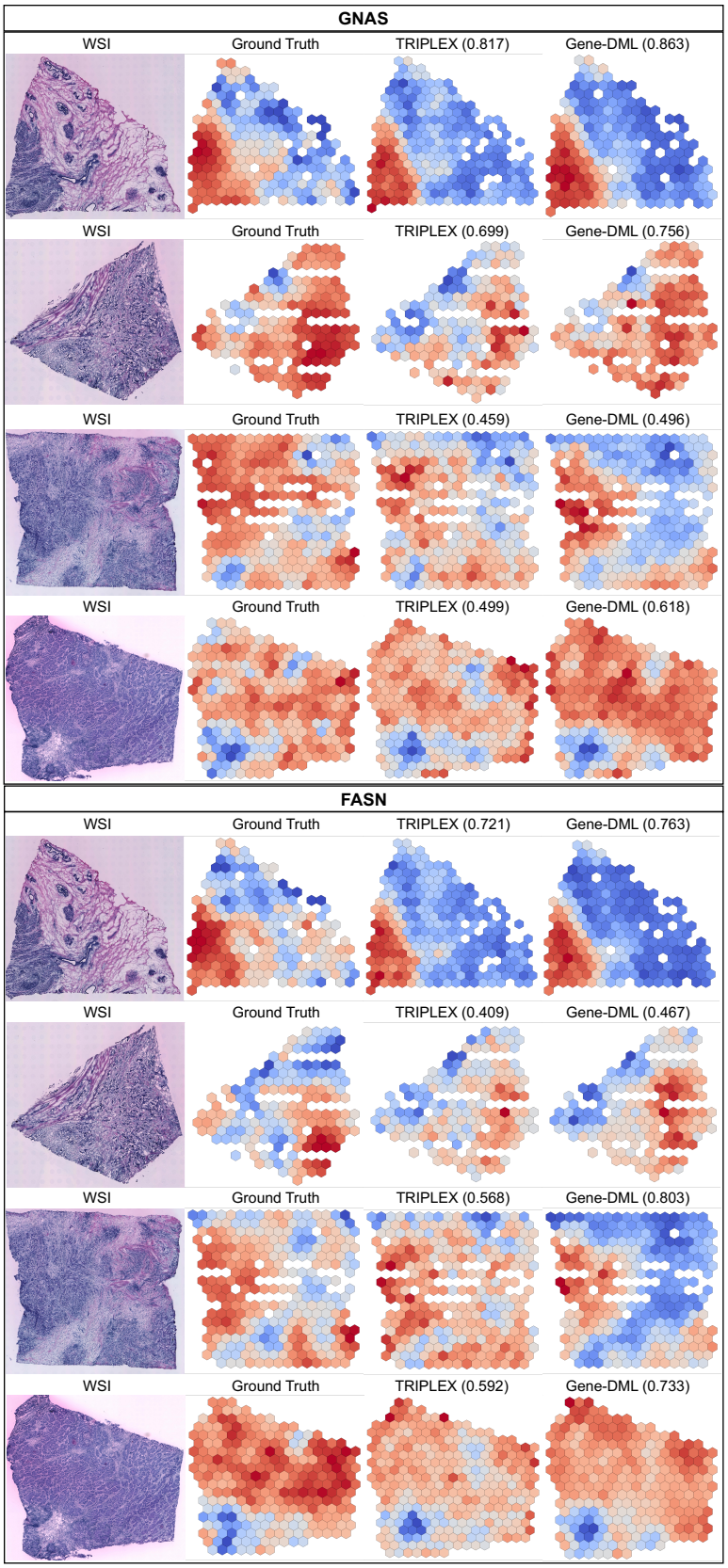


Figure 1. Visualization of cancer biomarker genes GNAS and FASN prediction on the dataset HER2ST.

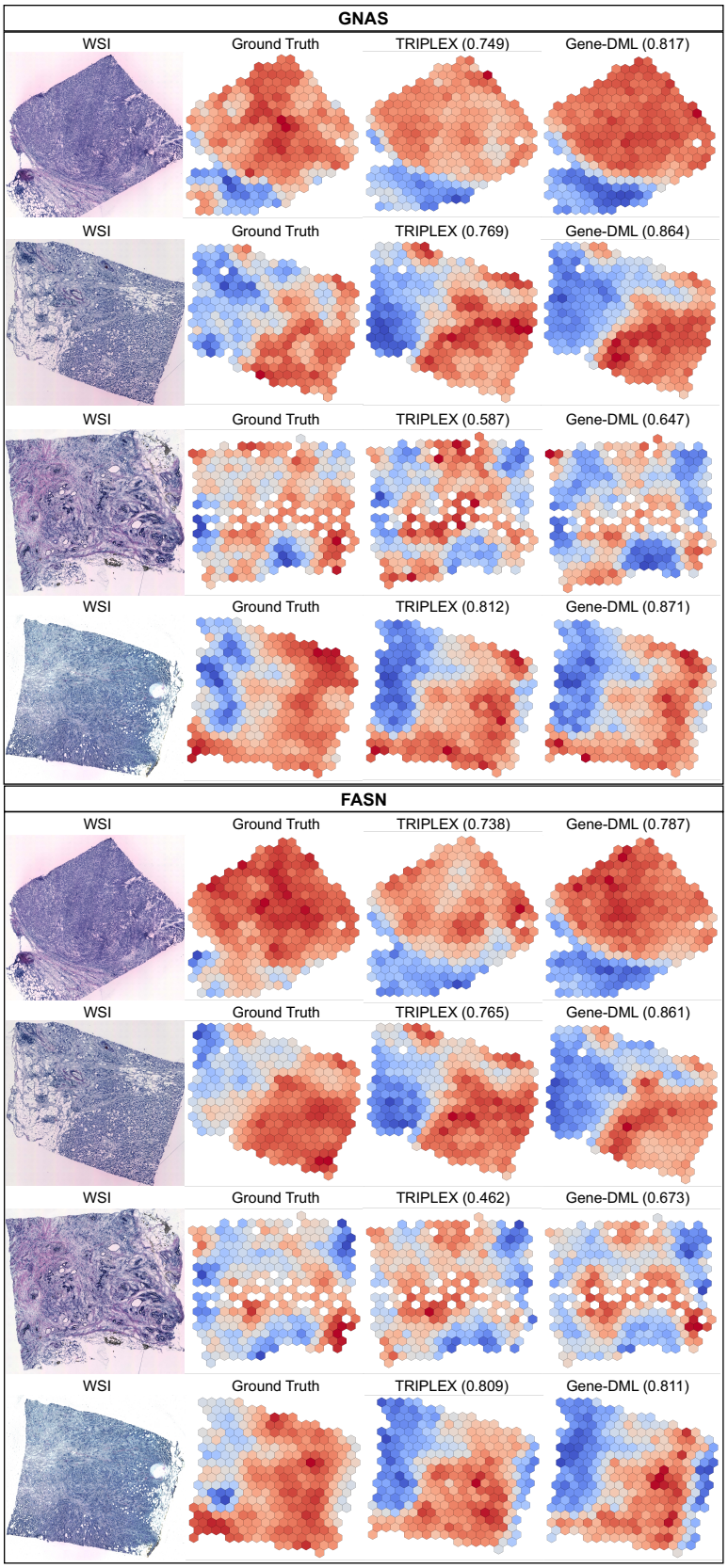


Figure 2. Visualization of cancer biomarker genes GNAS and FASN prediction on the dataset STNet.

| HER2ST |
| --- |
| IGKC, TMSB10, ERBB2, IGHG3, IGLC2, IGHA1, GAPDH, ACTB, IGLC3, IGHM, SERF2, PSMB3, PFN1, ACTG1, KRT19, RACK1, MUCL1, CISD3, APOE, MIEN1, SSR4, CALR, PSAP, CTSD, FTL, FTH1, TPT1, PTPRF, UBA52, P4HB, BEST1, HLA-B, FAU, SLC9A3R1, FN1, COL1A1, EEF2, IGHG4, CALML5, CD74, B2M, FASN, S100A9, MGP, CFL1, PSMD3, IGHG1, HLA-A, S100A6, MYL6, COL1A2, PHB, TAGLN2, HLA-E, HLA-C, KRT7, CD63, SYNGR2, STARD3, PABPC1, GPX4, GRB7, SLC25A6, AEBP1, GNAS, NDUFB9, EDF1, CRIP2, DDX5, OAZ1, EIF4G1, LMNA, GNB2, CST3, PCGF2, SDC1, S100A11, PRDX1, GRINA, ATP6V0B, TFF3, HLA-DRA, EEF1D, AZGP1, PPP1CA, FLNA, COL3A1, ATP5E, SPDEF, AP000769.1, ALDOA, PLXNB2, TAGLN, TUBA1B, APOC1, PRRC2A, LAPTM5, PTMS, KRT18, IFI27, PLD3, ADAM15, C1QA, AES, TSPO, MLLT6, TAPBP, SCAND1, ATP1A1, CD81, SEC61A1, CLDN3, PPDPF, S100A14, BGN, C3, MZT2B, S100A8, MDK, PFDN5, H2AFJ, SH3BGRL3, ENO1, XBP1, CYBA, COX6B1, TRAF4, CD24, PRSS8, MMP14, MUC1, VIM, MIDN, SPINT2, BST2, TIMP1, GUK1, ACTN4, CTSB, COX4I1, CCT3, HNRNPA2B1, SEPW1, LY6E, SCD, HSPB1, EIF4G2, BSG, ZYX, TUBB, LASP1, CD99, COL6A2, H1FX, RALY, UBE2M, SPARC, ATG10, HSP90AB1, ORMDL3, LMAN2, CHCHD2, COX7C, ARHGDIA, VMP1, UBC, IGFBP2, COPE, NUPR1, PERP, KRT81, PPP1R1B, LGALS3BP, SSR2, KIAA0100, MYL9, CIB1, IDH2, STARD10, LGALS1, COX6C, GRN, MAPKAPK2, GNAI2, KDELR1, COL18A1, UQCRQ, COX5B, ELOVL1, CHPF, CLDN4, C12orf57, LGALS3, HSP90AA1, JUP, A2M, NDUFB7, PGAP3, HSPA8, TCEB2, PEBP1, COPS9, ATP5G2, ATP6AP1, MYH9, LSM4, COX8A, UQCR11, ATP5B, DHCR24, PTBP1, EIF3B, NDUFA3, FKBP2, MMACHC, RABAC1, ISG15, PTMA, RRBP1, POSTN, C1QB, BCAP31, PSMB4, LAPTM4A, INTS1, FNBP1L, JTB, NBL1, HM13, SLC2A4RG, ROMO1, SERINC2, NDUFA11, RHOC, TXNIP, TYMP, NACA, HSP90B1, SNRPB, PFKL, VCP, ERGIC1, NUCKS1, PSMD8, CALM2, AP2S1, DBI, C4orf48, SDF4, TPI1 |

Figure 3. 250 Genes for the dataset HER2ST.

| STNet |
| --- |
| RPS3, IGLL5, RPLP1, TFF3, RPS18, GAPDH, TMSB10, RPLP2, RPS14, RPL37A, RPS19, RPL28, KRT19, RPL8, RPL13, RPL19, ACTB, RPL36, RPL18A, RPL35, RPL18, RPS2, RPS12, RPS21, RACK1, RPL13A, CTSD, FTL, PFN1, MGP, RPS15, RPS11, RPS16, HLA-B, UBA52, NHERF1, RPS17, PSAP, RPLP0, SERF2, RPS27, RPS8, RPL27A, MUC1, RPS28, H2AJ, RPL10, CALR, RPS29, RPL38, RPL11, P4HB, RPS6, CST3, FTH1, RPS4X, SSR4, RPL30, ERBB2, APOE, AZGP1, RPL3, COX6C, HLA-C, FAU, RPS9, EEF2, B2M, RPS5, RPL12, ACTG1, RPS27A, RPL37, RPL23, HLA-A, RPL31, RPL29, RPL7A, IFI27, PABPC1, CD74, BEST1, RPL32, FASN, S100A9, GPX4, RPL15, RPL27, MZT2B, RPL23A, HSPB1, MALAT1, RPS24, COL1A1, C4B, KRT18, CFL1, CD81, ALDOA, RPL35A, SYNGR2, PPP1CA, HLA-E, TAGLN, RPL9, CD63, RPS3A, LGALS3BP, IGFBP2, BST2, TPT1, EDF1, RPS25, ATP6V0B, TAPBP, GRINA, XBP1, S100A11, NBEAL1, AEBP1, CCND1, OAZ1, RPL14, TAGLN2, FN1, PPDPF, BCAP31, IFITM3, PRDX1, BGN, GNAS, PTMA, UBC, MZT2A, SLC25A6, RPS20, HSP90AB1, RPS10, MYL6, CLDN3, ATP6AP1, PRDX2, RPL24, GNB2, RPL34, RPL4, LMNA, NDUFA13, HLA-DRA, SNHG25, TIMP1, H1-10, RPS23, COX8A, KRT8, LY6E, ENO1, GRN, PTPRF, RPL7, UBB, BSG, ELOB, COX6B1, TMSB4X, C1QA, PRSS8, RPL5, UQCR11, RPS7, A2M, RPS15A, VIM, S100A6, NDUFA11, PSMD3, EVL, APOC1, H3-3B, ATP5F1E, PLXNB2, MYL9, TUBA1B, CTSB, ISG15, FLNA, RPS13, NDUFB9, EIF4A1, POLR2L, CYBA, CRIP2, EEF1D, ATP1A1, ELF3, TUFM, SH3BGRL3, STARD10, C3, GUK1, ZNF90, C12orf57, TLE5, SEC61A1, SDC1, PLD3, SPDEF, ARHGDIA, IFI6, LAPTM5, RPL41, CLU, GNAI2, PFDN5, RPL39, SSR2, COX4I1, RHOC, JUP, EIF4G1, FXYD3, TSPO, UQCRQ, COL1A2, RPL10A, S100A8, SELENOW, TPI1, ATP5MC2, PTMS, IGFBP5, LGALS1, SPINT2, RPSA, GSTP1, CHCHD2, EIF5A, COX5B, ATG10, RPL6, EEF1A1, CAPNS1, LMAN2, UBE2M, SPARC, EIF3C, GAS5, TUBB, ACTN4, IGFBP4 |

Figure 4. 250 Genes for the dataset STNet.

| skinST |
| --- |
| S100A8, KRT6A, KRT14, S100A9, KRT5, KRT6B, KRT16, KRT6C, KRT17, MT-CO3, S100A7, MT-CO2, SFN, S100A2, MT-CO1, ACTB, PERP, SPRR1B, KRT10, KRT1, EEF1A1, RPLP1, LGALS7B, LGALS7, COL1A1, FABP5, RPS12, HLA-B, MT-ND4, RPLP2, ACTG1, GJB2, B2M, TPT1, RPL13, MT-ATP6, RPS24, PFN1, KRTDAP, RPS6, DMKN, RPLP0, MT-ND3, RPL37A, DSP, CXCL14, RPS18, RPS17, RPS8, RPL13A, MT-CYB, RPL11, RPL27A, RPL28, MT-ND1, RPS27, RPL32, CSTA, RPL34, RPL31, COL1A2, RPL8, SBSN, TMSB10, ENO1, RPS14, RPL36, SPRR2A, RPL39, GSTP1, RPS27A, JUP, RPS19, RPL37, RPL27, RPL3, RPS29, COL3A1, RPS11, CSTB, RPL9, RACK1, ANXA2, RPL7A, RPL23, RPL19, S100A11, RPS2, RPS28, EEF2, ANXA1, CD74, PABPC1, LDHA, RPS3, RPL35A, DSC2, AQP3, RPS25, IFI27, CALML5, YWHAZ, RPL6, TMSB4X, RPS23, RPL12, S100A14, RPS4X, UBA52, SLPI, PKP1, RPL38, HLA-A, RPS13, LY6D, RPL24, ATP1B3, MYL6, GJB6, S100A6, HSPB1, RPL18, MT-ND2, SDC1, IVL, FTL, RPS3A, RPL10, RPS15A, PI3, RPL18A, S100A10, RPS7, S100A7A, RPL29, RPL26, RPL41, RPL4, RPL7, SPARC, VIM, PTMA, RPS20, MMP1, SH3BGRL3, RPL15, MYH9, GJA1, ITM2B, PPIA, RPL14, UBC, RPL5, CD44, AHNAK, RPL21, DSC3, CNFN, CD24, CFL1, COL17A1, HSP90AA1, RPS16, PKM, NACA, RPS5, ALDOA, H3F3B, S100A16, TAGLN2, HLA-C, TRIM29, LYPD3, FAU, LMNA, SPINK5, SPRR2E, RPL22, KRT2, CST3, DSG3, CLCA2, RPSA, DSG1, RPS9, NDRG1, AC090498.1, GRN, TXN, HSPA8, TGFBI, CTSB, SPRR2D, HLA-DRA, ACTN4, RPS21, EIF1, CTSD, ARPC2, CALML3, KLK7, CALM1, GNAS, DYNLL1, FLG, FLNA, DST, SLC2A1, PSAP, EIF4G2, EEF1B2, FGFBP1, LGALS1, ITGA6, MYL12B, TPI1, RPL10A, TMEM45A, BTF3, DSTN, RTN4, HNRNPA2B1, LAD1, ATP1A1, SERPINB3, PRDX1, COL6A1, ATP5E, PPDPF, TYMP, CD63, EIF5A, YWHAQ, PGK1, HLA-E, IFITM3, RPS26, IGFBP4, OAZ1, NPM1, LCE3D, FXYD3, MT2A, COL6A2, POLR2L, CD59, HNRNPK, RPL35, TMBIM6, HSP90AB1 |

Figure 5. 250 Genes for the dataset skinST.